$K\alpha$ x-ray satellite and hypersatellite spectra of vanadium metal and oxides excited in heavy-ion collisions

R. L. Watson, V. Horvat,* and Y. Peng
Cyclotron Institute and Department of Chemistry, Texas A&M University, College Station, Texas 77843-3366, USA
(Received 12 August 2008; published 3 December 2008)

The spectra of vanadium $K\alpha$ x rays excited in targets of vanadium metal, VO, V_2O_4, and V_2O_5 by 15 MeV/amu projectiles of Ne, Ar, Kr, Ag, and Ho have been measured with a curved-crystal spectrometer. The spectra were analyzed to extract the relative intensities and energies of $K\alpha$ satellites and hypersatellites emitted in the decay of states having single and double K vacancies, respectively, plus additional vacancies in the L shell ranging from zero to seven. The intensity distributions, energies, and hypersatellite to satellite intensity ratios were examined for chemical effects. The parameters of a "universal" scaling function were obtained for the description of $K\alpha$ x-ray hypersatellite intensity distributions excited by heavy-ion collisions in solid targets.

DOI: 10.1103/PhysRevA.78.062702 PACS number(s): 34.50.Fa, 32.30.Rj

I. INTRODUCTION

Previous studies have shown that the intensity distributions of $K\alpha$ x-ray satellites arising from the decay of collision-produced excited states containing single K-plus additional L-shell vacancies are sensitive to the chemical environment for elements in the second and third rows of the periodic table [1–5]. The origin of this chemical effect has been attributed to L vacancy transfer occurring between the time of collision and the time of x-ray emission. Both intra-atomic transitions from higher shells and interatomic transitions from neighboring atoms can significantly change the number of L vacancies present when a K x ray is emitted.

The key role of interatomic transitions in the L-vacancy filling process has been demonstrated by comparing $K\alpha$ x-ray satellite spectra for gaseous hydrides (e.g., SiH_4, H_2S, HCl) with spectra for more complex molecular gases containing the element of interest [3,4]. Additional evidence was deduced from the observation that the apparent degree of L-shell ionization displayed by the $K\alpha$ x-ray satellite intensity distributions of third-row solid compounds approximately correlates with the average valence electron density [1]. Perhaps the most dramatic effect of interatomic transitions on $K\alpha$ satellite spectra is the resonant behavior observed when the energy required to remove an electron from an energy level of a neighboring atom matches the energy released upon filling an L vacancy [5].

So far, similar chemical effects have not been reported for fourth-row elements. The valence shell of these elements is the N shell, which implies that L-vacancy transfer processes may be less sensitive to the chemical environment. However, chemical bonding in the fourth-row transition elements involves the $3d$ electrons and this fact has led to extensive investigations of the dependence on the oxidation state of their $K\beta$ x-ray structure excited by electrons, photons, and protons (see, for example, Refs. [6,7]). These studies have revealed significant changes in the relative intensities of the various $K\beta$ components.

In a recent study of the systematics of $K\alpha$ x-ray satellite distributions excited in (mostly) metallic targets by heavy ions spanning a wide range of energies and atomic numbers, it was found that the degree of L-shell ionization at the time of K x-ray emission, as represented by the experimental parameter p_L^x (the apparent average fraction of L vacancies), defines a universal curve when plotted versus the geometric model variable X_2 [8]. This finding provides an accurate means of comparing the p_L^x values for different chemical forms of a target element with that of the metal. The present work was undertaken with the primary objective of determining the extent to which the $K\alpha$ satellite and hypersatellite distributions of the fourth-row transition element vanadium depend on oxidation state. Measurements were performed for targets of vanadium metal, VO, V_2O_4, and V_2O_5 (having oxidation states of 0, +2, +4, and +5, respectively) bombarded by 15 MeV/amu beams of Ne, Ar, Kr, Ag, and Ho ions. Vanadium was chosen as the target element because the energy region covered by its K x-ray spectrum could be accessed with good resolution by second-order diffraction using a LiF crystal. In addition, its $K\alpha$ satellites and hypersatellites are all below the K absorption edge, and are well separated from each other, and from the $K\beta$ diagram and satellite peaks.

II. EXPERIMENTAL METHODS

Most of the experimental details were the same as those described in Ref. [8]. A 12.7 cm Johansson-type spectrometer with its focal circle oriented perpendicular to the beam axis was used to record x rays that underwent second-order diffraction from a curved LiF(200) crystal. The targets consisted of a 25.5 mg/cm^2 foil of metallic vanadium and thick compressed pellets of VO, V_2O_4, and V_2O_5. At least two spectra and usually three were taken for each combination of beam and target. The spectra were corrected for the efficiency of the detector (a flow proportional counter employing 90% argon and 10% methane), and for absorption and projectile energy loss in the target using the methods described in Ref. [2]. The relative number of emitted x rays in

*V-Horvat@tamu.edu

each x-ray energy interval $N_e(\varepsilon)$ was computed from the number of detected x rays $N_d(\varepsilon)$ using the formula

$$N_e(\varepsilon) = N_d(\varepsilon)\frac{\int_0^R \sigma(x)dx}{\varphi_{PC}(\varepsilon)\int_0^R \sigma(x)e^{-\mu(\varepsilon)x}dx}, \quad (1)$$

where φ_{PC} is the calculated efficiency of the proportional counter, $\sigma(x)$ is the K x-ray production cross section at distance x in the target, and μ is the mass attenuation coefficient (from Ref. [9]). The integrations were performed numerically over the range R of the projectile in the target. The values of $\sigma(x_i)$ were obtained using the expression

$$\sigma(x_i) = \sigma_0 - \int_0^{x_i} \frac{d\sigma}{dE}\frac{dE}{dx}dx, \quad (2)$$

where σ_0 is the K x-ray production cross section at the incident beam energy, and dE/dx is the projectile stopping power (from Ref. [10]). Both σ_0 and $d\sigma/dE$ were obtained using the semiempirical universal scaling function described in Ref. [11]. The average projectile energy for the detection of K x rays was obtained using the formula

$$\bar{E} = \frac{\int_0^R E(x)\sigma(x)\exp[-\mu(\varepsilon)x]dx}{\int_0^R \sigma(x)\exp[-\mu(\varepsilon)x]dx}, \quad (3)$$

where the projectile energy at distance x_i is given by

$$E(x_i) = E_0 - \int_0^{x_i} \frac{dE}{dx}dx. \quad (4)$$

A corrected spectrum obtained with 15 MeV/amu Kr ions incident on vanadium metal is shown in Fig. 1. The $K\alpha_{1,2}$ and $K\beta_{1,3}$ diagram peaks (thin solid green lines) were predominately excited by secondary electrons and x rays, while the major features of interest here, the satellite and hypersatellite distributions, were produced by heavy-ion collisions that created single K- plus additional L-vacancy (KL^n) states and double K- plus additional L-vacancy (K^2L^n) states, respectively. The spectra were fit with Voigt functions (shown by the dashed blue lines in Fig. 1) to extract the relative intensities and average energies of the peaks. The energy scale for each spectrum was determined from a linear calibration curve of wavelength versus channel number established by using the known wavelengths of the vanadium $K\alpha_{1,2}$ and $K\beta_{1,3}$ peaks (2.504 88 and 2.284 45 Å, respectively [12]) as calibration points.

The apparent average L vacancy fractions, p_L^x, defined by the expression

$$p_L^x = \frac{1}{8}\sum_{n=1}^{8}(nI_n/I_{tot}), \quad (5)$$

where

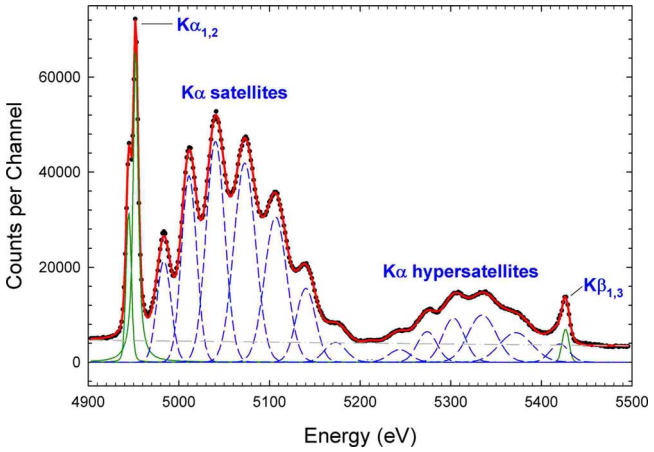

FIG. 1. (Color online) Spectrum of $K\alpha$ x rays from a vanadium metal target under bombardment by 15 MeV/amu Kr projectiles. The overall results of a least-squares fit using Voigt functions is shown by the thick solid (red) line. The $K\alpha_2$, $K\alpha_1$, and $K\beta_{1,3}$ diagram lines are shown by the thin solid (green) lines, while the satellite and hypersatellite peaks are shown by the thin dashed (blue) lines. The background is indicated by the dot-dashed (gray) line.

$$I_{tot} = \sum_{n=0}^{8} I_n, \quad (6)$$

were calculated directly from the measured satellite and hypersatellite relative intensities (I_n). In the case of the satellites, it was necessary to estimate the intensity of the collision-produced component of the KL^0 peak by fitting the rest of the satellite intensities to a binomial distribution. Another problem arises from the fact that the $K\alpha L^8$ and $K^2\alpha L^8$ peaks do not appear in the spectra since with eight vacancies in the L shell there are no electrons left to make a $K\alpha$ transition. Therefore, predicted intensities obtained from binomial fits to the observed satellite and hypersatellite distributions were used to represent I_8 in the calculation of p_L^x. However, inclusion of I_8 had a negligible effect on p_L^x for all cases except the hypersatellites excited by Kr, Ag, and Ho projectiles. The largest increase in p_L^x caused by the I_8 contribution was 2.9%.

III. RESULTS AND DISCUSSION

A. $K\alpha$ x-ray satellite and hypersatellite intensity distributions

The p_L^x values obtained for the vanadium $K\alpha$ satellites and hypersatellites are listed in Table I, along with the average beam energies for x-ray detection and corresponding values of the geometric model universal variable X_2 [calculated using Eq. (4) of Ref. [8]]. The $K\alpha$ x-ray satellite results are shown graphically in Fig. 2, where p_L^x is plotted versus X_2. Based on the work described in Ref. [8], the vanadium metal values were expected to lie on an empirical curve shown by the dashed (brown) line. The solid (blue) line was fit to the vanadium metal data points and shows very good agreement with the empirical curve. The relatively low p_L^x value data points for the vanadium oxides (obtained using Ne and Ar

TABLE I. Results of the $K\alpha$ satellite and hypersatellite intensity distribution analysis.

		$K\alpha$ satellites[a]			$K\alpha$ hypersatellites[b]		
Projectile	Target	$(E/M)_{ave}$ (MeV/amu)	X_2 (a.u.)	p_L^x	$(E/M)_{ave}$ (MeV/amu)	X_2 (a.u.)	p_L^x
$_{10}$Ne	V	14.58	1.170	0.121	14.56	1.171	0.158
	VO	13.28	1.213	0.128	13.09	1.219	0.146
	V_2O_4	13.14	1.217	0.128	12.93	1.225	0.159
	V_2O_5	13.11	1.218	0.130	12.91	1.226	0.152
$_{18}$Ar	V	13.69	2.162	0.271	13.60	2.163	0.329
	VO	12.57	2.228	0.285	12.36	2.242	0.364
	V_2O_4	12.42	2.238	0.284	12.21	2.252	0.359
	V_2O_5	12.40	2.240	0.288	12.18	2.255	0.355
$_{36}$Kr	V	12.91	4.412	0.439	12.76	4.431	0.590
	VO	11.85	4.555	0.433	11.65	4.584	0.596
	V_2O_4	11.72	4.574	0.457	11.53	4.602	0.585
	V_2O_5	11.70	4.577	0.430	11.57	4.605	0.591
$_{47}$Ag	V	12.29	5.870	0.476	12.11	5.899	0.628
	VO	11.56	6.002	0.466	11.38	6.037	0.630
	V_2O_4	11.48	6.017	0.461	11.32	6.048	0.631
	V_2O_5	11.48	6.017	0.465	11.31	6.050	0.638
$_{67}$Ho	V	12.81	8.235	0.514	12.69	8.264	0.692
	VO	11.42	8.594	0.494	11.24	8.645	0.674
	V_2O_4	11.31	8.625	0.500	11.14	8.673	0.669
	V_2O_5	11.31	8.625	0.511	11.14	8.673	0.673

[a]Estimated uncertainties in the satellite p_L^x values are $\pm 1.5\%$.
[b]Estimated uncertainties in the hypersatellite p_L^x values are $\pm 3.0\%$.

projectiles) are displaced from the corresponding vanadium metal data points due to differences in projectile energy loss, but they fall on the same curve. This indicates that the oxide satellite distributions are identical to those that would be obtained for vanadium metal using projectiles of the same average energy. However, the oxide p_L^x values obtained with the higher atomic number projectiles (i.e., Kr, Ag, and Ho) fall significantly and systematically below the curve defined by the metal data points. The dot-dashed (green) curve has been fit through the average p_L^x values of the oxides. All three fitted curves in Fig. 2 are logistic functions of the form

$$p_L^x = \frac{a}{[1 + (b/X_2)^c]}, \tag{7}$$

with parameter values of $a=0.5489\pm0.0072$, $b=2.201\pm0.046$, and $c=1.979\pm0.067$ for the metal curve and $a=0.5247\pm0.0064$, $b=2.087\pm0.041$, and $c=2.015\pm0.072$ for the oxide curve.

Although the effect is small, it may be concluded that, as the L vacancy fraction increases, the oxides become somewhat more efficient at filling L vacancies than the metal. This observation is consistent with the hypothesis expressed previously [1] that displacement of the valence electron density surrounding a target atom toward more electronegative neighboring atoms through chemical bonding lowers the probability that they will be ejected in a heavy-ion collision and increases the likelihood that they will be available for transfer to the multiply ionized target following the collision.

As mentioned in the Introduction, a previous study of chemical effects on the $K\alpha$ satellite distributions of third row compounds containing Al, Si, S, and Cl [1] revealed that the apparent average fraction of L vacancies decreases linearly with D_V, the average valence electron density, given by

$$D_V = N_A \frac{n_v \rho}{W}, \tag{8}$$

where N_A is Avogadro number, n_V is the total number of valence electrons per formula unit, ρ is the mass density, and W is the formula weight. The present data similarly displays a linear dependence on D_V, as is demonstrated in Fig. 3. The slope of the linear regression line that has been fit through the target p_L^x values for each projectile is displayed in this figure. It is evident that the slopes for the Ne and Ar projectile data are essentially zero while those for Kr, Ag, and Ho projectiles are negative and have magnitudes that are significantly greater than their uncertainties.

The results obtained for the $K\alpha$ x-ray hypersatellites are shown in Fig. 4. Unfortunately the low intensities of the hypersatellites and the accompanying larger error bars prevent as sensitive a test as was possible for the satellites. The solid (blue) curve shows a logistic function that has been fit to the vanadium metal data points (with $a=0.757\pm0.036$, $b=2.42\pm0.18$, and $c=1.90\pm0.20$). Within experimental error, it must be concluded that there is no difference between

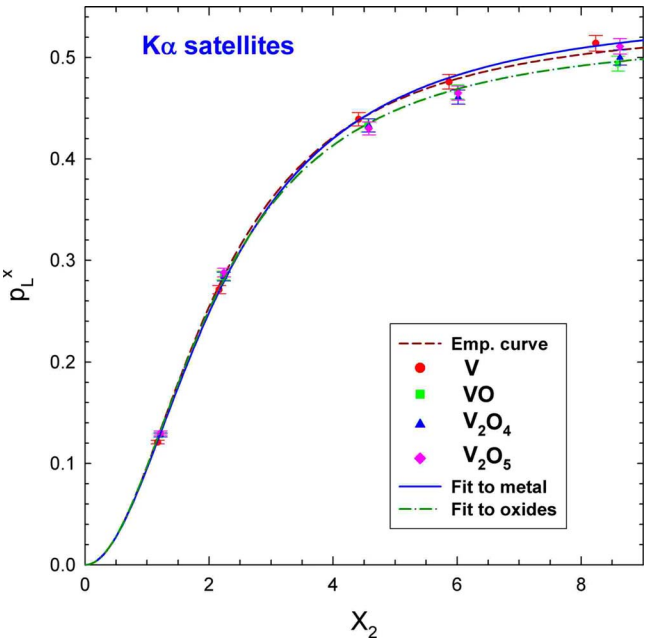

FIG. 2. (Color online) Apparent average L-vacancy fractions (p_L^x) obtained from the $K\alpha$ x-ray satellite intensity distributions of vanadium metal and oxides as a function of the geometric model variable X_2. Logistic functions have been fit to the data points for the metal [solid (blue) curve] and to the averages of the data points for the oxides [dot-dashed (green) curve]. The empirical curve from Ref. [8] is shown by the dashed (brown) curve.

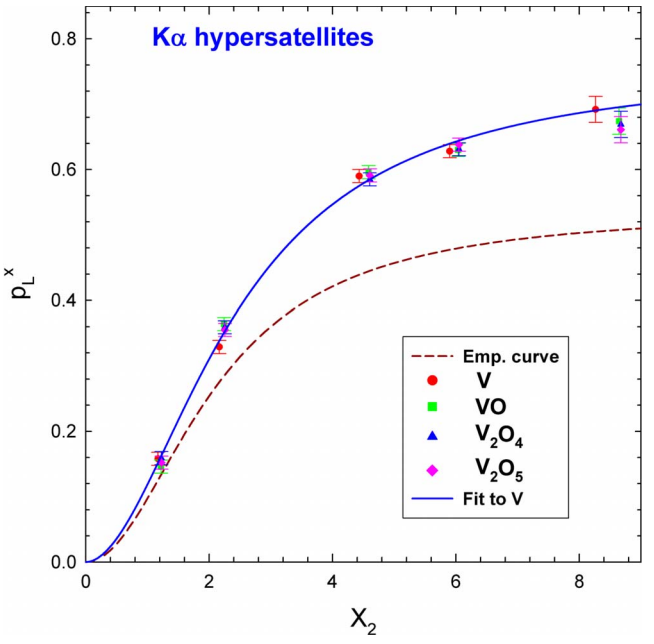

FIG. 4. (Color online) Apparent average L-vacancy fractions (p_L^x) obtained from the $K\alpha$ x-ray hypersatellite intensity distributions of vanadium metal and oxides as a function of the geometric model variable X_2. A logistic function has been fit to the data points for the metal [solid (blue) curve]. The empirical curve from Ref. [8] for the $K\alpha$ satellites is shown by the dashed (brown) curve.

the hypersatellite distributions of the metal and the oxides, with the possible exception of those excited by Ho projectiles. It is evident from a comparison of the vanadium hypersatellite curve with the dashed (brown) empirical satellite curve that, for solid targets, the p_L^x values of the hypersatellites are much larger than those of the satellites.

B. $K\alpha$ satellite and hypersatellite energies

The average energies of the $K\alpha$ satellite and hypersatellite peaks appearing in the spectra of vanadium metal and oxides are listed in Table II. Comparison of the energies for each target, excited by the same projectile indicated that any chemical shifts must be quite small, as is evidenced by the root-mean-square deviations listed for each peak. However, the energy of a given peak steadily increases with the projectile atomic number. In the past, this latter effect has been attributed to outer-shell ionization.

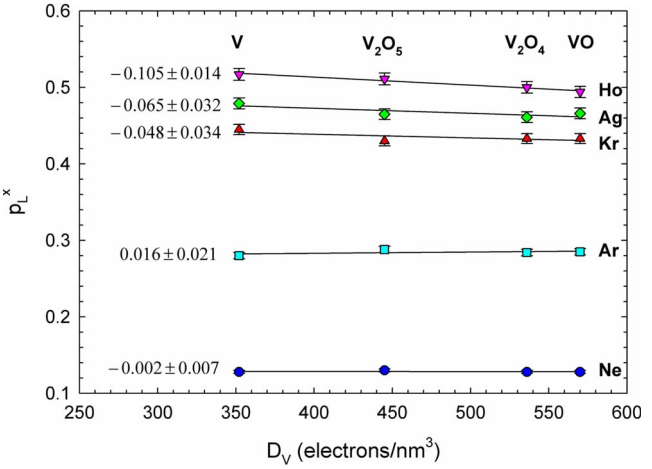

FIG. 3. (Color online) Graph showing the linear dependence of p_L^x on the average valence electron density D_V [Eq. (8)]. The numbers in the left-hand column are the slopes of the fitted straight lines in nm^3/electron.

The average energy shifts of the $K\alpha$ satellite peaks relative to the average $K\alpha_{12}$ diagram energy (4949.7 eV from Ref. [12]) are compared for each projectile in Fig. 5. Here, it is shown that the energy shifts observed with the different projectiles range between the energy shifts predicted by average-of-configuration Dirac-Fock calculations using the Desclaux program [13] for the outer-shell electrons all present (dashed purple curve) and all absent (dot-dashed green curve). Further details of the calculations are given in the Appendix. The same kind of graph is shown for the average energy shifts of the $K\alpha$ hypersatellite peaks relative to the average $K\alpha_{12}$ energy in Fig. 6. In the present work, the average Dirac-Fock energy shifts were obtained by averaging the calculated $K\alpha_1$ and $K\alpha_2$ transition energies

$$\bar{E}(K\alpha_{1,2}) = \frac{E(K\alpha_1) + RE(K\alpha_2)}{1+R}, \tag{9}$$

where R is the $K\alpha_2/K\alpha_1$ intensity ratio. In the case of the satellites, the value of R is expected to be close to the statistical value of 0.5 because a large number of transitions is possible for electron configurations containing a single K plus additional L vacancies (Scofield [14] calculated a theoretical value of 0.5082 for the $K\alpha$ diagram lines of vana-

TABLE II. Average energies of the vanadium $K\alpha L^n$ satellite and $K^2\alpha L^n$ hypersatellite peaks. The listed uncertainties are root-mean-square deviations from the average energies obtained for all four targets. The peak energies are subject to an additional ±0.5 eV uncertainty associated with inaccuracies in the energy calibrations due to possible chemical shifts of the diagram lines and energy shifts caused by collision-produced KL^0 contributions.

	Energies (eV)							
Projectile	$n=0$	$n=1$	$n=2$	$n=3$	$n=4$	$n=5$	$n=6$	$n=7$
				$K\alpha$ satellites				
Ne		4980.5 ± 0.2	5007.6 ± 0.8	5034.8 ± 0.7				
Ar		4982.4 ± 0.2	5009.7 ± 0.1	5037.6 ± 0.6	5066.9 ± 0.8	5098.9 ± 0.8		
Kr		4983.1 ± 0.6	5011.2 ± 0.5	5039.8 ± 0.6	5071.6 ± 0.7	5108.4 ± 0.8	5139.3 ± 0.7	5175.4 ± 1.6
Ag		4982.1 ± 0.4	5009.6 ± 0.2	5038.6 ± 0.3	5071.0 ± 0.6	5105.7 ± 1.1	5142.3 ± 0.6	5179.5 ± 0.6
Ho		4982.0 ± 0.3	5009.6 ± 0.2	5039.2 ± 0.9	5071.9 ± 0.3	5106.5 ± 0.9	5145.1 ± 0.3	5185.2 ± 0.5
				$K^2\alpha$ hypersatellites				
Ne	5181.3 ± 0.4	5207.5 ± 0.6	5236.3 ± 1.1	5263.9 ± 2.7				
Ar	5184.6 ± 0.7	5211.2 ± 0.7	5239.2 ± 0.6	5269.1 ± 0.4	5298.7 ± 1.2	5329.0 ± 2.5		
Kr		5212.6 ± 1.0	5243.8 ± 0.7	5273.4 ± 0.9	5302.2 ± 1.3	5333.8 ± 1.6	5371.6 ± 1.6	5417.3 ± 1.3
Ag			5242.6 ± 1.2	5271.3 ± 1.1	5301.6 ± 1.7	5337.0 ± 2.4	5376.8 ± 1.5	5417.8 ± 3.1
Ho			5244.0 ± 1.1	5272.7 ± 0.7	5302.0 ± 1.8	5336.0 ± 1.6	5379.1 ± 0.9	5421.4 ± 1.1

dium). The same holds true for the hypersatellites with $n > 0$. However, the K^2L^0 initial state configuration is a special case since, in the limit of LS coupling, only transitions to the $^1P_1$ final state are allowed. Hence, the $K\alpha_2$ transition is expected to be heavily favored. In the present analysis, the average energy for the K^2L^0 hypersatellite was computed using a theoretical R value of 10.1, from the calculations of Costa *et al.* [15].

It is reasonable to expect that the degree of outer-shell ionization should be related to the degree of inner-shell ionization, in which case the $K\alpha$ satellite and hypersatellite energy shifts should correlate with p_L^x. This was verified in Ref. [8] for a variety of targets and projectiles. Plots of the satellite and hypersatellite energy shifts as a function of p_L^x using the current vanadium data are shown in Figs. 7 and 8, respectively. In the present work, the straight line least-squares fits displayed in these figures were extrapolated to predict the limiting energy shifts as p_L^x approaches zero. These energy shifts (ΔE_0) are presumed to be the energy shifts that would be observed if all outer-shell electrons were present. The

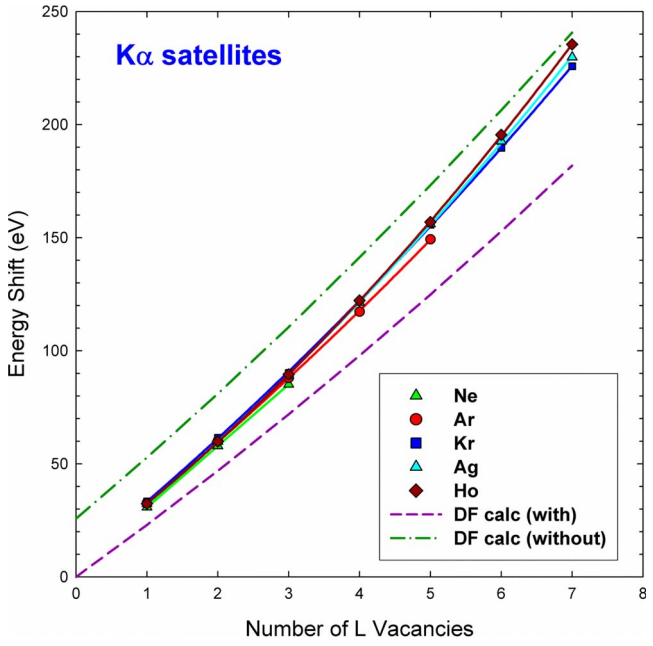

FIG. 5. (Color online) The $K\alpha$ satellite average energy shifts measured relative to the average $K\alpha_{1,2}$ diagram peak energy [Eq. (9)]. The dashed (purple) and dot-dashed (green) curves show the average Dirac-Fock energy shifts calculated for a vanadium atom with and without outer-shell electrons present, respectively.

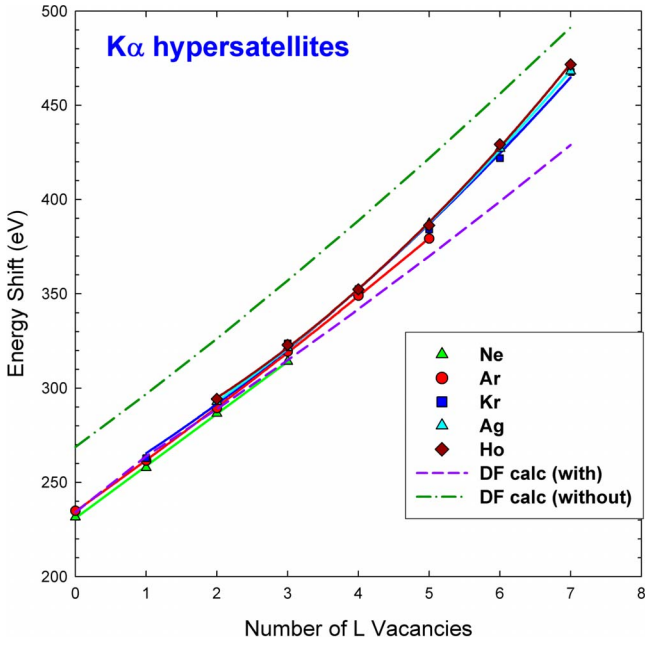

FIG. 6. (Color online) The $K\alpha$ hypersatellite average energy shifts measured relative to the average $K\alpha_{1,2}$ diagram peak energy [Eq. (9)]. The dashed (purple) and dot-dashed (green) curves show the average Dirac-Fock energy shifts calculated for a vanadium atom with and without outer-shell electrons present, respectively.

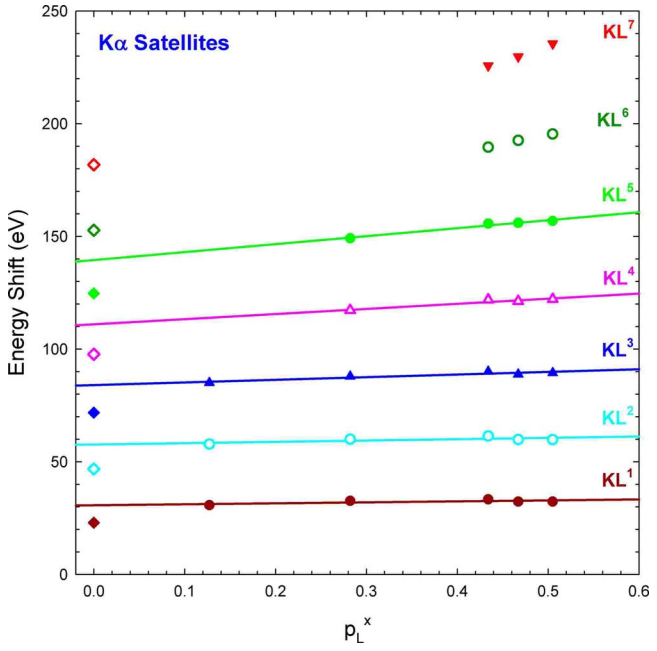

FIG. 7. (Color online) The $K\alpha$ satellite average energy shifts as a function of p_L^x. The results of straight line least-squares fits are shown by the solid lines and the average Dirac-Fock energy shifts calculated for vanadium atoms with all outer-shell electrons present are shown by the diamond-shaped data points at $p_L^x=0$.

calculated energy shifts for vanadium atoms with all outer-shell electrons present are shown by the diamond-shaped points in Figs. 7 and 8, and they are compared with the extrapolated energy shifts at $p_L^x=0$ in Table III. As may be seen from Fig. 7 and Table III, the calculated energy shifts for the $K\alpha$ satellites are systematically smaller (by 12–34%) than the experimental energy shifts. On the other hand, the agreement between the calculated (average-of-configuration Dirac-Fock) and experimental energy shifts is much better for the hypersatellites, with differences ranging from 2.8% to −1.0%.

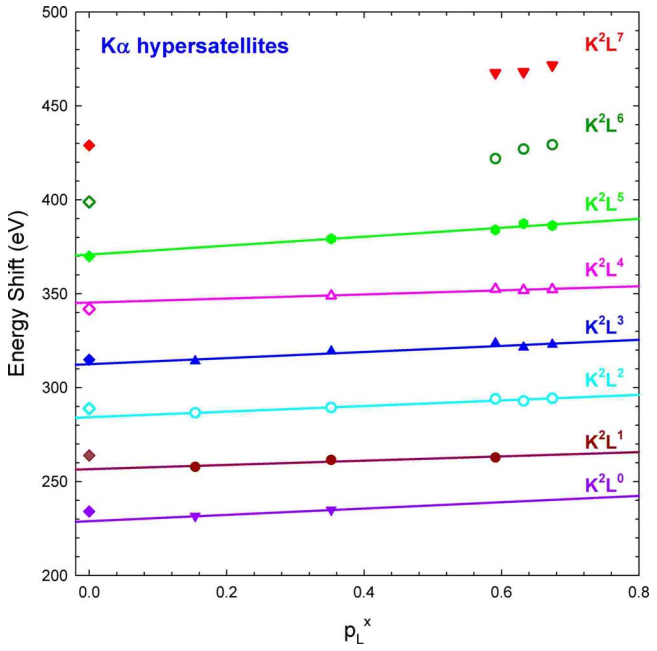

FIG. 8. (Color online) The $K\alpha$ hypersatellite average energy shifts as a function of p_L^x. The results of straight line least-squares fits are shown by the solid lines and the average Dirac-Fock energy shifts calculated for vanadium atoms with all outer-shell electrons present are shown by the diamond-shaped data points at $p_L^x=0$.

TABLE III. Comparison of the extrapolated $K\alpha L^n$ satellite and $K^2\alpha L^n$ hypersatellite energy shifts (ΔE_0; in eV) with theoretical predictions for vanadium atoms having all outer-shell electrons present.

	$(\Delta E_0;\ \text{in eV})_{\text{exp}}$		$(\Delta E_0;\ \text{in eV})_{\text{theo}}$	
n	This work	Other	This work[a]	Other
		Satellites		
1	30.8 ± 1.0		23.0	
2	57.7 ± 1.3		46.9	
3	84.0 ± 1.1		71.9	
4	111.1 ± 2.1		97.8	
5	139.5 ± 1.8		124.8	
6			152.8	
7			181.9	
		Hypersatellites		
0	229.0 ± 1.2	228 ± 2[b]	234.1	227.9[c]
				228.0[d]
1	256.6 ± 1.5		263.9	
2	284.3 ± 0.9		288.9	
3	312.6 ± 1.7		314.9	
4	345.3 ± 1.4		341.9	
5	370.8 ± 2.9		369.9	
6			398.9	
7			429.0	

[a]Average of configuration Dirac-Fock (see Appendix).
[b]From Ref. [16] [re-evaluated relative to $E(K\alpha_{1,2})$].
[c]Dirac-Fock with Breit interaction+QED from Ref. [15] [re-evaluated relative to $E(K\alpha_{1,2})$].
[d]Dirac-Hartree-Slater with Breit interaction from Ref. [17] [interpolated and re-evaluated relative to $E(K\alpha_{1,2})$].

The $K^2\alpha L^0$ hypersatellite is of particular interest since several authors have performed calculations for this case that take into account the Breit interaction [15,17,18] and include radiative corrections from the most recent QED calculations [15]. It is gratifying to find that the present extrapolated value of the average $K^2\alpha L^0$ hypersatellite energy shift is in good agreement with these calculations.

C. $K\alpha$ hypersatellite to satellite intensity ratios

The ratios of the integrated intensities of $K\alpha$ hypersatellites and satellites ($R_{H/S}$) for the various projectile and target combinations are listed in Table IV and plotted versus the projectile atomic number in Fig. 9. They do not appear to exhibit a dependence on the chemical composition of the target, although the intensity ratios for the metal obtained with Kr and Ag ions are significantly higher than those for the oxides.

TABLE IV. Ratios of the $K\alpha$ hypersatellite to satellite integrated intensities ($R_{H/S}$).

Projectile atomic number	Target			
Z_1	V	VO	V_2O_4	V_2O_5
10	0.072 ± 0.003	0.057 ± 0.004	0.082 ± 0.017	0.069 ± 0.001
18	0.173 ± 0.016	0.160 ± 0.010	0.150 ± 0.003	0.179 ± 0.004
36	0.214 ± 0.006	0.193 ± 0.005	0.183 ± 0.004	0.186 ± 0.004
47	0.280 ± 0.011	0.245 ± 0.005	0.241 ± 0.007	0.229 ± 0.020
67	0.202 ± 0.014	0.233 ± 0.009	0.212 ± 0.009	0.234 ± 0.012

The cross sections for single and double K-vacancy production may be expressed in terms of the number of $K\alpha$ x rays emitted in the decay of single and double K-vacancy states (N_K and N_{2K}, respectively) as

$$\sigma_K = \frac{N_K - N_K^*}{C_K} \quad \text{and} \quad \sigma_{2K} = \frac{N_{2K}}{C_{2K}}, \tag{10}$$

where N_K^* is the number of x rays emitted from single K-vacancy states formed in the decay of double K-vacancy states, and C_K and C_{2K} are factors containing the corresponding average $K\alpha$ fluorescence yields. If it is assumed that the average $K\alpha$ fluorescence yields for double and single K-vacancy states are approximately equal, then $N_K' \approx N_{2K}$ and

$$\frac{\sigma_{2K}}{\sigma_K} \approx \frac{N_{2K}}{N_K - N_{2K}} = \frac{R_{H/S}}{1 - R_{H/S}}. \tag{11}$$

In Fig. 9, it may be seen that the hypersatellite to satellite intensity ratios level off at a value of around 0.23, which [according to Eq. (11)] corresponds to a cross-section ratio of approximately 0.30.

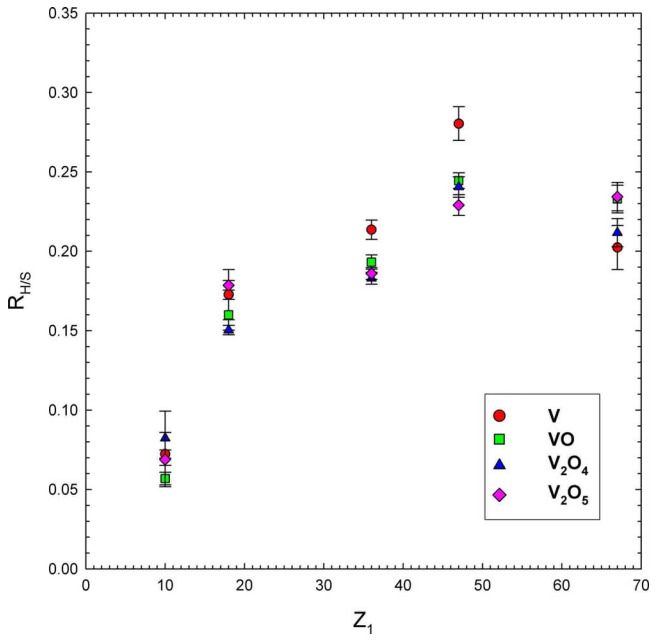

FIG. 9. (Color online) The ratio of the $K\alpha$ hypersatellite to satellite integrated intensity as a function of the projectile atomic number.

A simple model commonly has been used to estimate double to single K- and L-vacancy production cross-section ratios. It assumes the electrons are ejected independently with probabilities that may be expressed as binomial factors involving the single-electron ionization probability $p(b)$, where b is the impact parameter. Representation of $p(b)$ by an exponential function

$$p(b) = p_0 \exp(-b/r),$$

where p_0 and r are constants, leads to Eq. (6) of Ref. [19], which, in turn, yields the following:

$$\sigma_K = 4\pi^2 p_0 [1 - p_0/4],$$

$$\sigma_{2K} = (\pi/2) r^2 p_0^2. \tag{12}$$

Using these expressions, the double to single K-vacancy production cross-section ratio reduces to

$$\frac{\sigma_{2K}}{\sigma_K} = \frac{p_0}{2(4 - p_0)}. \tag{13}$$

This equation predicts a maximum value of only 0.17 (when $p_0 = 1$) for the cross-section ratio, which is far below the value predicted by Eq. (11). Apparently, some of the assumptions used in the derivation of Eqs. (11) and (12) are not valid for the high states of ionization produced with Kr, Ag, and Ho projectiles at 15 MeV/amu.

The most obvious factor that would lead to the observed disagreement is the ratio of the average fluorescence yields, which was assumed to be one in both derivations. Unfortunately, rigorous calculations of fluorescence yields for the decay of states having single and double K vacancies plus additional L vacancies have been carried out only for neon atoms [20–22]. Examination of the results of these calculations reveal that the double to single K-vacancy average fluorescence yield ratios for neon configurations having n L vacancies remain close to one for $n = 0-3$, but increases by nearly a factor of 2 in going from $n = 3$ to $n = 5$ (see Fig. 5 of Ref. [23]). In the present case, the fluorescence yield question is complicated even further by intra- and interatomic vacancy transfer. Another shortcoming of the above model used to derive Eq. (13) is the assumption that the same values of p_0 and r apply to both the single and double K-vacancy production cross sections.

IV. CONCLUSION

Measurements of the spectra of vanadium $K\alpha$ x rays emitted in collisions of 15 MeV/amu Ne, Ar, Kr, Ag, and Ho projectiles with metal and oxide targets have provided detailed information concerning the intensities and energies of the $K\alpha$ x ray satellites and hypersatellites. The dependence of the apparent average L-vacancy fraction of vanadium metal on the geometric model variable X_2 was in good agreement with an empirical "universal" (logistic function) curve determined previously [8]. A similar curve determined for the oxides deviated significantly from the curve for the metal at $X_2>4$, indicating that the rates of L-vacancy transfer for the oxides somewhat exceed those for the metal at high values of p_L^x. Furthermore, the p_L^x values of the metal and the oxides were found to correlate linearly with the average valence electron density in a manner similar to that observed previously for third-row elements [1].

The p_L^x values obtained for the hypersatellites were well represented by a logistic function and provided the parameters of an empirical universal curve for the description of hypersatellite distributions excited in heavy-ion collisions with solid targets. The measurements indicate that the satellite and hypersatellite distributions are nearly identical at $X_2<1.5$, but at higher values of X_2 the p_L^x values of the hypersatellites rapidly rise above those of the satellites and are higher by about 33% at $X_2=8$. No obvious dependence on chemical environment was evident in a comparison of the hypersatellite data for the metal and the oxides, although the p_L^x value of the metal obtained with Ho projectiles was substantially larger than those for the oxides.

An examination of the average energies of the satellite and hypersatellite peaks did not reveal any dependence on chemical environment. Extrapolation of the linear relationship between peak energy and p_L^x provided estimates of the satellite energies for vanadium atoms with all outer-shell electrons present. The energy shifts measured relative to the average $K\alpha_{1,2}$ diagram peak energy were compared with average-of-configuration Dirac-Fock calculations. Rather poor agreement (within 12–34 %) was found for the satellites, while much better agreement (2.8–1.0 %) resulted for the hypersatellites. The experimental energy shift for the $K^2\alpha L^0$ peak agreed well with the results of theoretical calculations that included the Breit interaction and QED corrections.

Finally, the $K\alpha$ hypersatellite to satellite intensity ratios were analyzed for possible chemical effects. Although the ratios for the metal appeared to be anomalously high for the spectra excited by Kr and Ag projectiles, the ratios for the rest of the projectiles were in agreement within experimental error. A simple model for predicting the ratio of double K-vacancy to single K-vacancy production cross sections from the $K\alpha$ hypersatellite to satellite intensity ratio was found to be inadequate. It was concluded that it is not valid to assume the average fluorescence yields of the hypersatellites and satellites are equal for the highly ionized states produced under the present experimental conditions.

APPENDIX: CALCULATIONS OF $K\alpha$ SATELLITE AND HYPERSATELLITE ENERGY SHIFTS

The multiconfiguration relativistic Dirac-Fock program of Desclaux [13] was used to calculate each transition energy as a difference between the total atomic energy of the initial electronic configuration and the total atomic energy of the final electronic configuration. The initial electronic configurations included all combinations of $1s^i2s^j2p_{1/2}^k2p_{3/2}^m3s^23p_{1/2}^23p_{3/2}^43d_{3/2}^43d_{5/2}^34s^2$, where $i=0$ for the hypersatellite transitions and $i=1$ for the satellite transitions. The total number of L electrons in the initial configuration is $n_e=j+k+m$. The corresponding final electronic configurations had one more $1s$ electron as well as one less $2p_{1/2}$ electron (for the $K\alpha_2$ transitions) or one less $2p_{3/2}$ electron (for the $K\alpha_1$ transitions). For any given transition type (i.e., $K\alpha_1^S$, $K\alpha_1^H$, $K\alpha_2^S$, or $K\alpha_2^H$), the transition energies corresponding to the same n_e were averaged assuming a purely statistical probability in the initial electronic configuration, i.e.,

$$E(n_e)=\frac{\sum_{j,k,m} w(j,k,m)E(j,k,m)}{\sum_{j,k,m} w(j,k,m)}, \tag{A1}$$

where

$$w(j,k,m)=\binom{2}{j}\binom{2}{k}\binom{4}{m}. \tag{A2}$$

The summations in Eq. (A1) include only those terms for which $j+k+m=n_e$ and also $k>0$ (for the $K\alpha_2$ transitions) or $m>0$ (for the $K\alpha_1$ transitions). The calculations were done for one electronic configuration at a time (thus neglecting configuration interaction), averaging over all contributing terms in the given configuration. Similar calculations were also done for the $1s^i2s^j2p_{1/2}^k2p_{3/2}^m$ initial configurations, in which the M and N electrons are absent.

ACKNOWLEDGMENTS

This work was supported by Research Grant No. A355 from the Robert A. Welch Foundation.

[1] R. L. Watson, T. Chiao, and F. E. Jenson, Phys. Rev. Lett. **35**, 254 (1975).
[2] R. L. Watson, A. K. Leeper, B. I. Sonobe, T. Chiao, and F. E. Jenson, Phys. Rev. A **15**, 914 (1977).
[3] F. Hopkins, A. Little, N. Cue, and V. Dutkiewicz, Phys. Rev. Lett. **37**, 1100 (1976).
[4] J. A. Demarest and R. L. Watson, Phys. Rev. A **17**, 1302 (1978).
[5] O. Benka, R. L. Watson, and R. A. Kenefick, Phys. Rev. Lett. **47**, 1202 (1981).
[6] S. D. Gamblin and D. S. Urch, J. Electron Spectrosc. Relat. Phenom. **113**, 179 (2001).
[7] S. Fazinić, M. Jaskšić, L. Mandić, and J. Dobrinić, Phys. Rev. A **74**, 062501 (2006).

[8] V. Horvat, R. L. Watson, and Y. Peng, Phys. Rev. A **74**, 022718 (2006).
[9] J. H. Hubbell and S. M. Seltzer, http://physics.nist.gov/PhysRefData/XrayMassCoef/cover.html
[10] F. Ziegler, SRIM, http://www.srim.org/
[11] R. L. Watson, Y. Peng, V. Horvat, and A. N. Perumal, Phys. Rev. A **74**, 062709 (2006).
[12] R. D. Deslattes, E. G. Kessler, Jr., P. Indelicato, L. deBilly, E. Lindroth, and J. Anton, Rev. Mod. Phys. **75**, 35 (2003).
[13] J. P. Desclaux, Comput. Phys. Commun. **9**, 31 (1975).
[14] J. H. Scofield, Phys. Rev. A **9**, 1041 (1974).
[15] A. M. Costa, M. C. Martins, J. P. Santos, P. Indelicato, and F. Parente, J. Phys. B **40**, 57 (2007).
[16] O. Keski-Rahkonen, J. Saijonmaa, M. Suvanen, and A. Servomaa, Phys. Scr. **16**, 105 (1977).
[17] M. H. Chen and B. Crasemann, Phys. Rev. A **25**, 391 (1982).
[18] B. Boschung, J.-Cl. Dousse, B. Galley, Ch. Herren, J. Hoszowska, J. Kern, Ch. Rhême, Z. Halabuka, T. Ludziejewski, P. Rymuza, Z. Sujkowski, and M. Polasik, Phys. Rev. A **51**, 3650 (1995).
[19] V. Horvat, R. L. Watson, J. M. Blackadar, A. N. Perumal, and Y. Peng, Phys. Rev. A **71**, 062709 (2005).
[20] C. P. Bhalla and M. Hein, Phys. Rev. Lett. **30**, 39 (1973).
[21] M. H. Chen and B. Crasemann, Phys. Rev. A **12**, 959 (1975).
[22] C. P. Bhalla, J. Phys. B **8**, 2787 (1975).
[23] R. L. Watson, O. Benka, K. Parthasaradhi, R. J. Maurer, and J. M. Sanders, J. Phys. B **16**, 835 (1983).